



# Glass-Steel Triangulated Structures: Parametric Nonlinear Finite-Element Analysis of In-Plane and Out-of-Plane Structural Response of Triangular Laminated Glass Panels

Francesco Laccone<sup>1</sup>; Christian Louter<sup>2</sup>; and Maurizio Froli<sup>3</sup>

**Abstract:** Glass exhibits brittle failure behavior. Therefore, redundancy is a fundamental design requirement when using glass as a main structural material. On this basis, a novel structural concept has been developed for hybrid glass-steel posttensioned triangulated structures, where the two materials collaborate. In forming such lattice structure, local fracture must be avoided. This paper presents a parametric study that highlights the influences of mechanical and geometrical parameters on the in-plane and out-of-plane static behaviour of laminated triangular glass panels. The resulting data set constitutes a useful source for the designer to select the most appropriate component. The main sensitivity parameters are panel length, laminate thickness, and interlayer stiffness. DOI: 10.1061/(ASCE)AE.1943-5568.0000374. © 2019 American Society of Civil Engineers.

**Author keywords:** Structural glass; Hybrid glass-steel structure; Triangular glass pane; Tetrahelix; Buckling; Long-spanned; Posttensioning.

## Introduction

In the last decades, the use of glass as a structural material has increased considerably. Driven by transparency and its apparent sense of lightness, such material satisfies the quest for dematerialization in contemporary architecture. However, as is well known, glass exhibits brittle behavior and high scatter tension strength. In order to avoid sudden collapses caused by high stresses, static fatigue, and accidental damages, the rules of fail-safe design (FSD; Haldimann et al. 2008) are adopted. In addition, hybridism provides a further safety margin.

Because primary all-glass structural elements usually lack ductility, except the quasi-ductile behavior inherent in laminated panels, research efforts have focused on several static concepts based on glass-steel collaboration. These range from composite beams (Martens et al. 2015a; Louter et al. 2012; Martens et al. 2016a, b) to arched (Sobek 2007; Weller et al. 2009) or vaulted structures (Weller et al. 2008, 2010; Ioannis et al. 2012).

In analogy with posttensioned concrete elements, prestress has been more recently introduced in glass structures (Martens et al. 2015b), practiced by bonded (embedded or glued) components (Louter et al. 2014; Cupac et al. 2017; Bedon and Louter 2017) or unbonded external tendons (Jordão et al. 2014; Feng et al. 2015;

Engelmann and Weller 2016; Bedon and Louter 2016). The aim is to add additional tensile strength to glass for safer postbreakage behavior.

The current paper is framed in the research context of posttensioned segmented glass-steel structures and focuses on a specific concept, *Travi Vitree Tensegrity* (TVT), developed at the University of Pisa for building long-span beams (Froli and Lani 2010; Froli and Mamone 2014; Mamone 2015) and frames (Froli et al. 2014, 2017). TVT is based on the principles of FSD, foremost hierarchy, segmentation, and redundancy.

TVTs comprise two segmented mutually connected webs, where triangular glass panels are arranged in a Warren scheme. Panel corners are clamped into monolateral steel nodes by means of posttensioned bars, which secure contact at the interface of the two materials, allowing detachment in case the prestress rate is overcome. Full-scale experiments showed calibrated ductile failure: the yielding of the lower bars always preceded the buckling of the glass within a hierarchical chain of ruptures. Segmentation and component doubling allow TVTs to withstand external loads with a reduced safety factor even in the case of accidental failure of some panels. Dry assembly (without bolts and adhesives) makes replacement cost-effective. A photo of the third TVT prototype, TVT<sub>γ</sub>, spanning 12 m, is shown in Fig. 1.

In the development of long-spanned and tall lattice structures, redundancy is indeed an essential requirement. Therefore, because it is not possible to benefit from a parallel assembly of webs as in TVTs, a novel alternative static concept (Froli and Laccone 2018c) has been developed to create volume-forming envelopes, free-form façades, or roofs. The static concept is based on the collaboration of multiple laminated flat glass panels with a filigree steel truss.

Enhanced redundancy with respect to state-of-the-art static concepts was stated in Froli and Laccone (2018c) on two example structures by means of simplified global finite-element models (FEMs). The next step, and the subject of the present research, is to focus on local failure modes. The ultimate limit state (ULS) of in-plane-loaded and out-of-plane-loaded triangular laminated glass panels was investigated by means of three-dimensional (3D) nonlinear finite-element analyses (FEAs) using ANSYS Release

<sup>1</sup>Research Fellow, Dept. of Energy, Systems, Territory, and Construction Engineering, Univ. of Pisa, Largo L. Lazzarino, Pisa 56122, Italy; Institute of Information Science and Technologies “A. Faedo”–National Research Council of Italy, Via Giuseppe Moruzzi 1, Pisa 56124, Italy (corresponding author). ORCID: <https://orcid.org/0000-0002-3787-7215>. Email: francesco.laccone@destec.unipi.it; francesco.laccone@isti.cnr.it

<sup>2</sup>Assistant Professor, Dept. of Architectural Engineering and Technology, Faculty of Architecture and the Built Environment, TU Delft, Delft 2628 BL, Netherlands. ORCID: <https://orcid.org/0000-0003-2131-4351>

<sup>3</sup>Professor, Dept. of Energy, Systems, Territory, and Construction Engineering, Univ. of Pisa, Largo L. Lazzarino, Pisa 56122, Italy.

Note. This manuscript was submitted on March 7, 2018; approved on March 28, 2019; published online on November 21, 2019. Discussion period open until April 21, 2020; separate discussions must be submitted for individual papers. This paper is part of the *Journal of Architectural Engineering*, © ASCE, ISSN 1076-0431.



**Fig. 1.** Third example of segmented hybrid glass-steel TVT beams: 12-m-span TVT $\gamma$ .

version 16.2 to highlight the influences of key geometrical and mechanical parameters. A conveniently modular tetrahelical tower was selected to derive reference design values.

### Structural Concept and Geometry

The static concept is based on earlier experimental tests made on full-scale TVT prototypes. More specifically, the structural system (Fig. 2) consists of several flat glass panels connected to a slender steel frame. Spatial steel nodes merge three to six beams and house monolateral dry recesses that clamp the panel corners. External posttensioned cables are fixed at the nodes and transfer prestress to the structure. The main points and structural principles of the static concept are briefly stated as follows:

- The ideal continuous curve-shaped surface is segmented, generating multiple triangular (or in general polygonal) flat glass panels, in compliance with FSD and constituting a low-maintenance, cost-saving strategy because only broken panels need to be replaced once failed.
- Mutual prestress of the components is applied by means of external cables. This is done to globally stiffen the system and to additionally apply a beneficial compression prestress. A design opportunity is to orient the cable path based on loading condition.

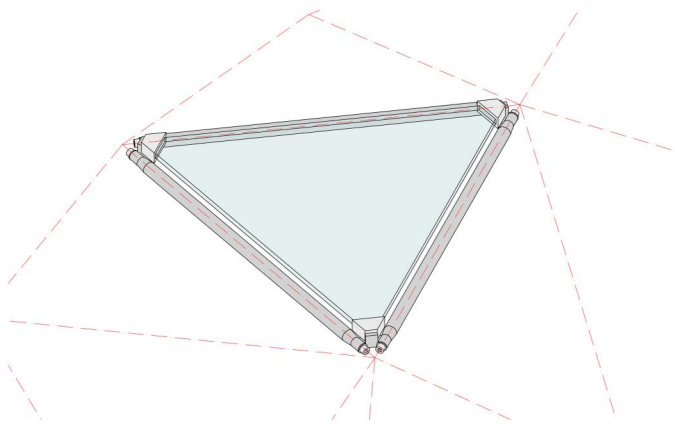


**Fig. 2.** Schematic of base unit of investigated hybrid glass-steel system.

- The dry assembly of the connection allows easy mounting and replacement of the components. Because only contact ensures the transfer of forces, the panel can slide within the connection in case of tensile stresses greater than precompression values.
- In the way just described, the panel is mostly compressed except for tension stresses that may arise from significant second-order effects or out-of-plane loadings.
- The steel beams that form the metal skeleton frame are set adjacent to the panels' edges and collaborate with the glass in supporting loads. The frame additionally constitutes a suitable redundancy barrier before ULS collapse and so is designed to withstand at least its own weight in the absolute worst case where all glass panels are accidentally cracked and so mechanically useless. Lastly, the metal skeleton facilitates assembly and replacement, avoiding the use of provisional scaffolding.

The structural principles apply to self-supporting volume-generating structures. To this end, a particularly convenient geometry category, triangulated solids, is adopted. Among these, triangulated helical polyhedrons (Kappraff 2001; Pottmann 2007) are one of the most promising for enhancing modularity, and their inherent geometric properties may be additionally exploited for structural purposes [Figs. 3(a–c)]. Triangulated helical polyhedrons are cylinders decomposed into all-equal equilateral triangular faces, whose vertices lie on the base cylindrical surface. The edges of adjacent triangles draw polygonal paths that are dual of cylindrical helices on the cylinder can be drawn by iteratively joining consecutive edges of adjacent triangles—hence, the name. For each solid outer surface, it is possible to identify three groups of parallel helical spirals characterized by different slopes with respect to the horizontal plane.

The installation of a hybrid structure on triangulated surfaces provides for flat glass panels in place of triangular faces and a for steel truss at panels' edges. Such a triangulated frame is inherently statically determinate with six-way stiff connections. Glass panels provide a noticeable stiffening contribution in compressed areas of the structure, reducing the structural role of the frame itself. Additionally, the helical polylines are optimal paths for external posttensioned cables.

The smallest and simplest triangulated helical polyhedron is the tetrahelix [Fig. 3(c)], selected as a reference case study for its similarity with a cantilever hollow cylindrical beam. The term *tetrahelix* was first introduced by Fuller (1982) because its form can be regarded as a vertical assembly of tetrahedrons with each one sharing a face with another one [Fig. 3(d)].

In the hybrid tetrahelix (Fig. 4), the glass collaborates with a steel filigree truss, whose nodes are six-way connections except for the ground and upper nodes, where connectivity is reduced. The nodes are the crucial part of the system, constituting the location of the anchoring part of both the beam end extremities and the panel vertices. The posttensioned cables are also point-fixed at the outer side of each node.

Effective prestress paths overlap the most inclined group of helical polylines. Their mechanical role is to confer on the panel in-plane precompression and additionally to equip the structure for radial confinement, vertical compression, and global stiffening. Global analysis results are provided in Froli and Laccone (2018a, b).

Local safe breakage is obtained using double-laminated equilateral triangular glass panels, and, as in a TVT system, the panel corners are rounded to avoid stress concentration and are confined in a dry-clamped steel casing. To obtain a monolateral restraint, neither bolted nor adhesive connections are introduced on the glass. Only compression forces, by contact, can propagate from the steel truss to the panel. Moreover, the panel can slide in the direction of

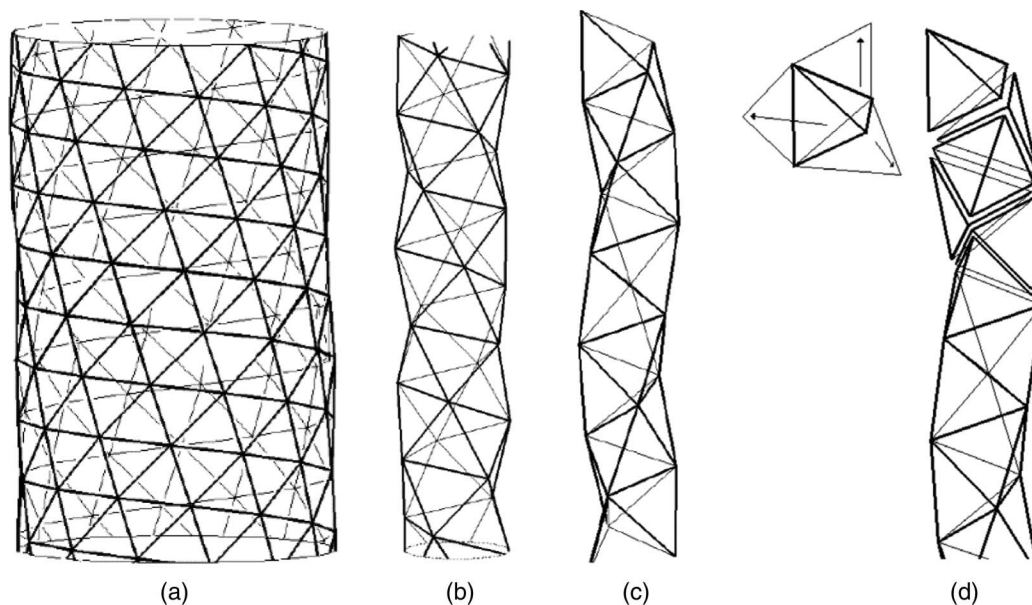


**Fig. 3.** Triangulated solids: (a–c) helical polyhedrons; and (d) genesis of tetrahelix geometrical form.

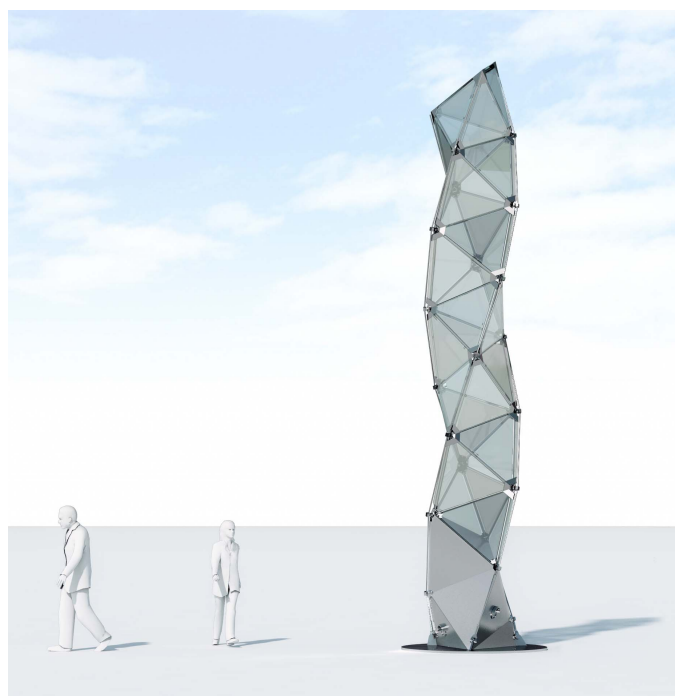


**Fig. 4.** Seven-meter-tall hybrid glass-steel tetrahelix.

the bisector line of the corner angle to avoid undesired tension stresses. For this reason, the posttensioned triangular panel may be sensitive to compressive forces, leading to buckling due to its slenderness. Tensile failure may also occur because of bending for an out-of-plane load. This is why the main conservative load cases selected for analysis were

- Nonlinear progressive buckling of an in-plane symmetrically loaded panel; in a single-layer lattice structure, local buckling is relevant because it can cause fracture;
- Nonlinear static analysis for an out-of-plane-loaded panel, where fracture occurs when tensile strength limits in the bent glass panel are reached.

Laminated triangular glass panels with clamped corners as part of a lattice structure have not been investigated experimentally or numerically. TVT panels, although the closest structural component to these panels in terms of boundary conditions and geometry, present different loading conditions: being web panels of beams, their own weight represents in-plane loading as well as posttensioning load; out-of-plane loads are negligible.

Several researchers have addressed the in-plane and out-of-plane behavior of large glass panes. In particular, rectangular plate is an active research area because it is extensively adopted in floor-to-floor façades (Silvestru et al. 2013; Enghardt 2007; Enghardt and Bergmeister 2005; Huvener et al. 2007; Wellershoff 2006; Haarhuis and Wever 2016; Štrukelj et al. 2015; Stepinac et al. 2013) and insulating glass units (Memari et al. 2003). Even though similarity exists in loading and boundary conditions, the structural system and the shape of the panels play a substantial mechanical role. Consequently, the present study, a first step in the analysis of these panels, adopted the methodology of parametric nonlinear finite-element (FE) investigations.

## Materials and Method

### Parameters

The effects of mechanical and geometrical parameters were investigated via geometrically nonlinear FEA on a double-laminated triangular panel with rounded corners. In each analysis, only one parameter was varied while the others were kept invariant as reference values. Fig. 5 shows the configuration and key parameters investigated: panel side length  $L$ , glass thickness  $t_g$ , interlayer shear modulus  $G_i$ , interlayer thickness  $t_i$ , and initial imperfection of the panel  $u$ . Table 1 summarizes the parameter values assumed in the analyses. The reference values were  $L = 1,000$  mm,  $t_g = 8$  mm,  $G_i = 300$  MPa,  $t_i = 1.52$  mm, and  $u = 0$  mm.

Side lengths were spaced from 500 mm to a maximum 3,000 mm—well within the limits of typical commercial sizes (i.e.,  $6 \times 3.21$  m). The reference 1,000-mm-sided panel was the one adopted in the design of the structure in Fig. 4 and in Froli and Laccone (2018a, b). For  $t_g$ , the nominal values of 4, 6, 8,

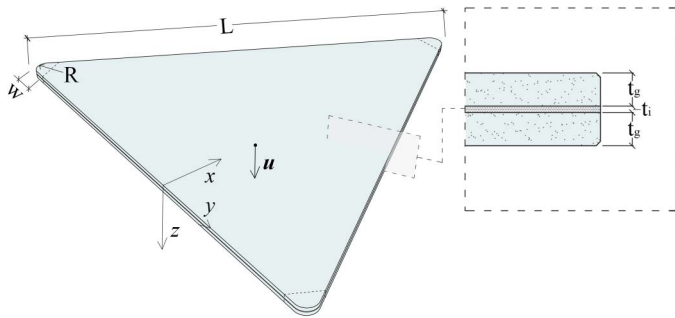


Fig. 5. Triangular panel: geometrical parameters.

Table 1. Parameters varied in nonlinear analyses

Parameter	Notation (unit)	Values
Side length	$L$ (mm)	500, <b>1,000</b> , 1,500, 2,000, 2,500, 3,000
Glass thickness	$t_g$ (mm)	4, 6, <b>8</b> , 10, 12, 15
Interlayer thickness	$t_i$ (mm)	0.38, 0.76, <b>1.52</b>
Interlayer shear modulus	$G_i$ (kN/mm <sup>2</sup> )	0.1, 1, 10, 70, 150, <b>300</b> , 600
Initial imperfection	$u$ (mm)	<b>0</b> , $L/1,000$ , $L/400$ , $L/100$ , $L/50$

Note: Reference values are in bold.

10, 12, and 15 mm were chosen in line with commercially available thicknesses. For the interlayer, thickness values of 0.38, 0.76, and 1.52 mm were assumed. In order to simulate the effects of viscosity as well as the various interlayer polymers, different values for shear modulus were assumed but, as a simplification, both glass and interlayer polymers were considered linear elastic isotropic despite their evident nonisotropic behavior.

The reference value of 300 MPa characterized a stiff polyvinylbutyral (PVB) interlayer with a low load duration at room temperature (Eastman 2017; Kuraray Europe 2017). Other values adopted in the parametric investigation represented various load durations and temperature as well as other interlayer polymers (for instance SentryGlas and Trosifol ExtraStiff).

As yet there has been no systematic evaluation of imperfection in 2D large plates; both imperfection amplitude  $u$  and shape were therefore unknown. Amplitude  $u$  was expressed as the maximum of the imposed field of deformation, and its absolute value was a fraction of the side length of the panel. For other structural components, the following values were considered:  $L/1,000$ , which Amadio and Bedon (2010), Mocibob (2008), and others introduced when studying rectangular panels;  $L/400$ , which Belis et al. (2011) recommended as a characteristic design value after processing experimental measurements on 312 monolithic and laminated beam-like panels; and  $L/100$  and  $L/50$ , which were chosen to determine the tendency of the numerical curve. The value of  $L/50$  is not within production tolerance. Concerning imperfection shape, a parabola was adopted for all simulations as suggested by Belis et al. (2011). Cylindrical and spherical inelastic deformation fields were considered, but the obtained ultimate load was always larger than the parabola. Eigenmodes, which are usually considered for buckling studies, provided conservative values as well. Their resulting shape was stiffened because of the presence of clamping areas.

The materials used in the numerical models followed constitutive linear stress-strain law. The properties of the glass (soda, lime,

Table 2. Mechanical properties in numerical models

Mechanical properties	Notation (unit)	Glass	Interlayer
Density	$\rho$ (kg/m <sup>3</sup> )	2,500	1,070
Young's modulus	$E$ (N/mm <sup>2</sup> )	70,000	Variable
Poisson's coefficient	$\nu$	0.23	0.45

silica) and the interlayer (typical PVB values) were derived from Haldimann et al. (2008) and are summarized in Table 2.

## Method

The static scheme of the studied panel is shown in Fig. 6(a). Corners were provided with compression-only in-plane support, while the out-of-plane clamping restraint was modeled as an elastic support [Fig. 6(b)].

The two load cases (in plane and out of plane) were computed in a two-phase analysis (Fig. 7). In the first phase, the structure was simulated without external loads to mimic positioning of the panel on the truss and its posttensioning. Two loads applied in this phase: dead load, which was directly computed from the material properties of the panel layers, and posttensioning load, regarded as a self-balanced group of free-body forces. In order to maximize dead load gravity  $g$  and to decouple its effect from that of in-plane loading, the gravity direction was set normal to the midsurface plane. As a consequence, because the dead load was out of plane, the resulting deformation (in Phase 1) acted like a geometric imperfection for the loading to follow.

For all analyses, the contribution of dead load was assumed to always be present, even if it was not highlighted in the resulting graphs. Particularly in the imperfection sensitivity analysis, the deformed shape at the end of Phase 1 should be read as the superimposition of dead load deformation and initial imperfection displacement field.

The overall structural behavior of a hybrid tetrahelix tower had been investigated in a global analysis by Froli and Laccone (2018a, b), from which the ratio of loads acting on a single panel was deduced. Posttensioning loading and cable layout were responsible for vertical and radial confinement of the structure. Only the most inclined helices of the base polyhedron were equipped with cables. Three continuous cables were used. Posttensioning was not carried out along all edges but only on one for each panel. That edge was subjected to a main compressive loading flux adjacent to the external cable path and a minor isotropic confinement in the orthogonal direction.

Based on the results of the global analysis, the external forces in Phase 1 were derived to reproduce these effects: a main component was parallel to the BC edge of the triangle ( $y$ -axis), and a minor load was oriented perpendicularly ( $x$ -axis). The A vertex gave the equilibrium reaction.

For simplicity in describing the behavior of laminated triangular glass panels, the load magnitude was disassociated from the effects of the tower aspect ratio and the cable posttensioning rate. Therefore, the two Phase-1 external load components were set to differ by one order of magnitude,  $F_1 = 10$  kN and  $F_2 = 1$  kN, respectively.

Two separate analyses were directly linked to the Phase-1 results and simulated the two critical live loads of Phase 2. For in-plane loading, the lowest external force able to buckle the panel was configured as posttensioning loading. This load scheme was represented as uniformly increasing up to failure by the coefficient  $\lambda$ . The final value of  $\lambda$  was defined as the nonlinear buckling multiplier

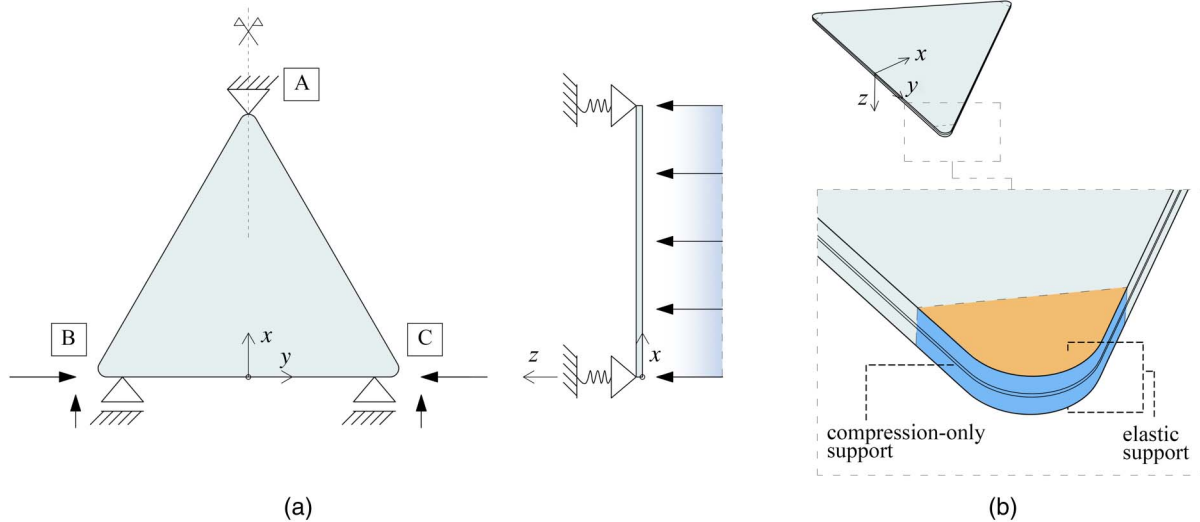
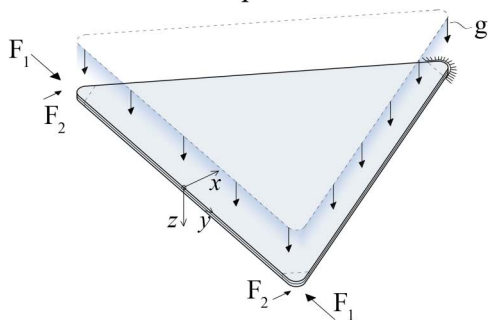
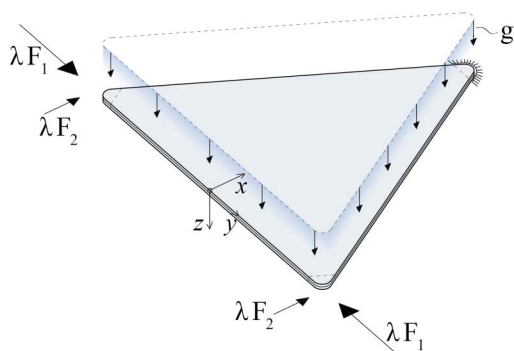


**Fig. 6.** Modeling of panel: (a) static scheme; and (b) boundary conditions.

**Phase 1: dead load and pre-stress**



**Phase 2: in-plane loading**



**Phase 2: out-of-plane loading**

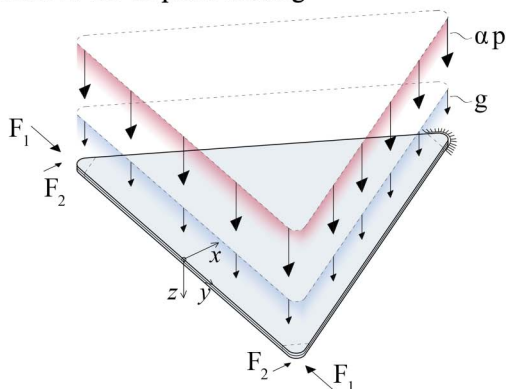


**Fig. 7.** Loads on panels: Phases 1 and 2 for each load scenario.

$$\lambda = \frac{F_{cr}}{F_1}$$

where  $F_{cr}$  = snap-through value of each geometrically nonlinear analysis, manually identified from the load-displacement graph when the following condition occurred:

$$\frac{F_n - F_{n-1}}{u_n - u_{n-1}} \leq \delta$$

where  $F_n$  ( $F_{n-1}$ ) and  $u_n$  ( $u_{n-1}$ ) = force and maximum out-of-plane deflection at the  $n$ th ( $n - 1$ ) load step; and  $\delta = 0.1$ , identifying a low slope segment in the force-displacement curve.

For out-of-plane loading, a specific uniform pressure of  $p = 1.0 \text{ kN/m}^2$  was applied on the surface of the  $z = 0$  face of the laminated panel and its coefficient  $\alpha$  was increased to register the peak of the maximum principal stress. Based on the  $\alpha$  values of the out-of-plane load multiplier, tension stress isolines were derived. This strategy to highlight the range of stresses avoid the introduction of a specific glass strength, which was a function of treatments and processing, environmental factors, and probability distribution. Long-term effects associated with posttensioning losses were neglected in this study.

**Modeling Strategy and Analysis**

The geometry of the equilateral triangular laminated panel was generated from a parametric 3D solid model, in which all key geometric parameters were scalable. The size of the clamping area—namely, its depth  $w$  and the radius  $R$  of the rounded panel corners (Fig. 5)—was also scaled with respect to the parameter  $L$  and met the mechanical and technological requirements of force transfer.

A full solid FE model was realized through discretization of the imported three-layer solid geometry by means of three-dimensional FEs exhibiting quadratic displacement behavior (SOLID186 and SOLID187) and three degrees of freedom per node. The mid-side node avoided susceptibility to any shear locking that may have occurred because of its low height-to-width ratio—for instance, in the discretization of the interlayer. All materials were set as elastic isotropic according to the previous hypothesis.

The mesh pattern was produced using a hex-dominant method. Its maximum size was determined based mesh sensitivity analysis [Fig. 8(a)] and panel side length  $L$ . The latter was indeed

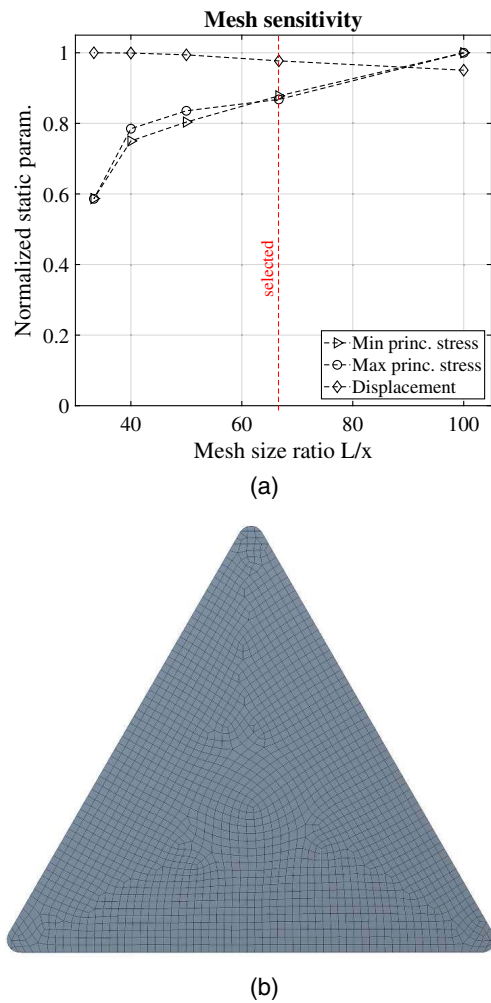


**Fig. 8.** FE mesh: (a) sensitivity analysis; and (b) typical mesh pattern on  $L = 1,000$ -mm panel.

proportional to the  $w$  and  $R$  dimensions, which in turn governed the accuracy of the solution at the corners because loading and constraint conditions were set there. Therefore, the ratio between the panel side length and the mesh maximum size ( $L/x$ ) assumed the

value of 50 for the 500-mm-sided panel, 66.7 for the 1,000-mm-sided panel, and up to 150 for larger panels. A typical mesh pattern is shown in Fig. 8(b). Generally, only one solid FE was used for the thickness of each layer except in panels thicker than 10 mm, such as the double 15-mm-thick 500-mm-edge side panel, where an additional thickness subdivision was applied in order to improve bending stress results and deformation accuracy.

To simulate a perfectly bonded interface between all layers, contact elements CONTA174 were used. Such an interface would not allow any relative movement or interpenetration between the solids.

To comply with the static scheme in Fig. 6(a), boundary conditions were applied at the corners: the faces orthogonal to the midplane were equipped with nonlinear compression-only normal supports; the upper and lower faces of all corners had elastic supports—a bed of springs with a specific stiffness of  $k = 85 \text{ kN/mm}^2$  derived from the moment-curvature plot obtained by means of a geometrically nonlinear detailed FEA of the clamping device. For this purpose, the spacer material, technology, and methodology used by Froli and Lani (2010), Froli and Mamone (2014), and Mamone (2015) were used. The spacers had significance for the behavior of panels with a limited load introduction area, as noted by Ebert (2014). In the present study, to avoid tension peaks, 2-mm-thick EN AW 6060 T5 aluminium alloy meeting CNR DT 208/2011 specifications (CNR 2011) and having almost the same Young's modulus as that of glass, was used for spacers at the interface between the glass and the steel.

External loads were applied as remote forces in the models. To avoid nonrealistic distortions, only glass faces were loaded. For large deformations, a two-step geometric nonlinear analysis was run for each model. Despite the parametric model-building strategy, the results were manually verified with a nonlinear solver. Recurring displacement fields on the Phase-2 panels are shown in Fig. 9.

## Results and Discussion

In this section, the results of the numerical analyses are summarized and the effects of the different parameters are discussed. For the in-plane load case, the results are shown in a plot of the nonlinear buckling multiplier  $\lambda$  versus the parameters (Figs. 10–13); for the out-of-plane load case, the magnitude of surface pressure

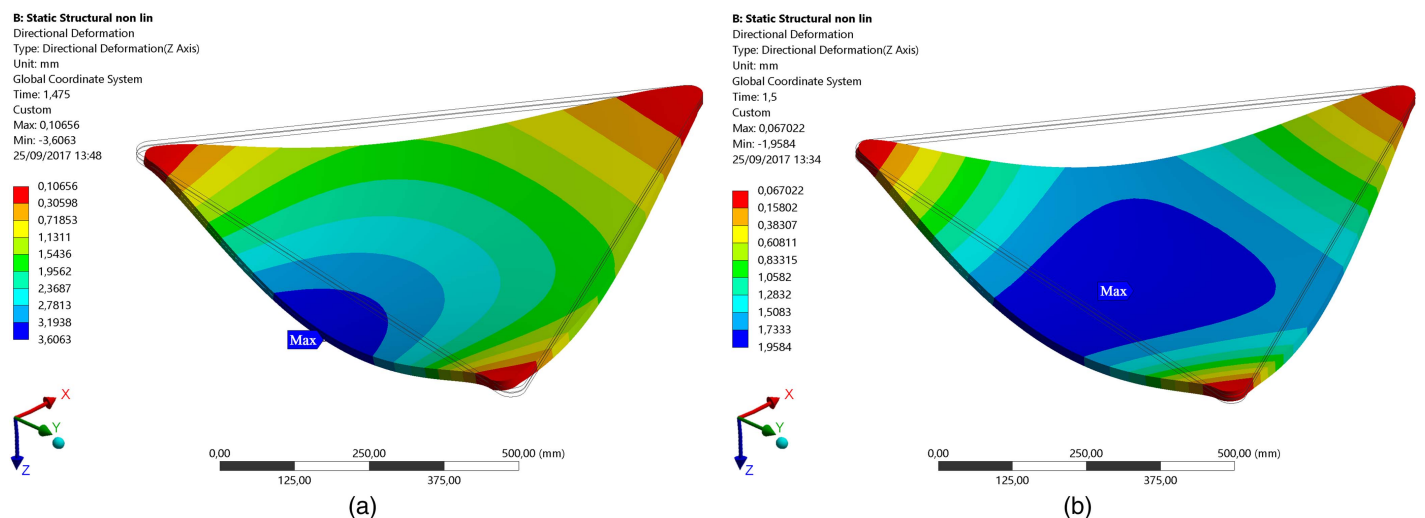


**Fig. 9.** Displacement field for reference glass panel: (a) in-plane load; and (b) out-of-plane load.

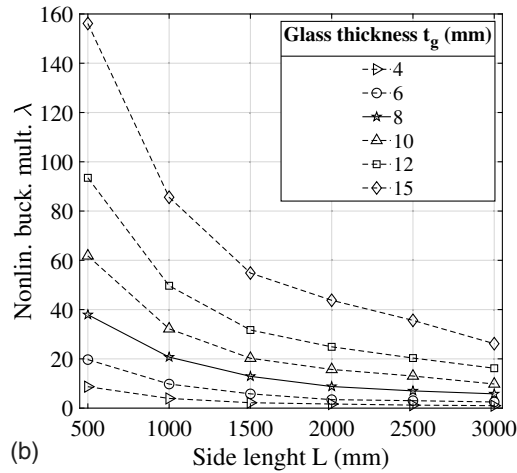
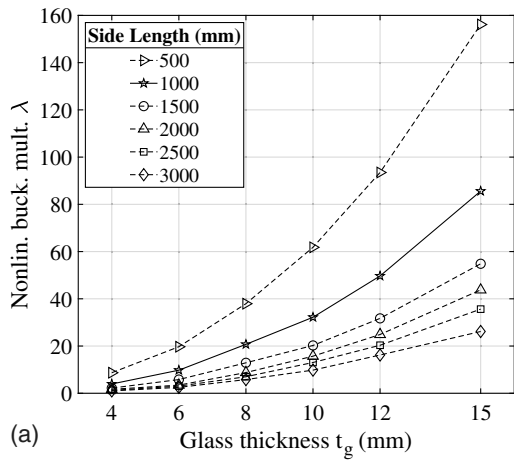


**Fig. 10.** Nonlinear buckling multipliers for in-plane loading: effect of (a) side length; and (b) glass thickness.

$\alpha \times p$  versus the sensitivity parameters is plotted (Figs. 11–17). Reference values are represented by continuous lines marked by symbols.

### In-Plane Loading

#### Effect of Side Length and Glass Thickness

The side length of the panel and the thickness sensitivity of both laminate glass components are depicted in Fig. 10. Because slenderness is the governing parameter for stability problems, special attention was paid to its effect on the ultimate buckling multiplier  $\lambda$ ; all possible combinations of glass thickness and side length were evaluated using the 3D domain shown in Fig. 11.

From Fig. 10(a), it is seen that, concerning the effect of side length, the buckling multiplier exponentially grows with increasing glass thickness: the smaller the panel, the higher the exponent of the ideal fitting curve. Negative exponential functions are shown in Fig. 10(b), where the thinner the component pane, the flatter the interpolating curve of the buckling multipliers. Glass thickness and panel side length exhibit a larger influence on the mechanical response of predominantly in-plane-loaded panels with clamped edges. The border curve of the progressive buckling failure domain is an exponential 3D function.

#### Effect of Interlayer Stiffness

Time behavior, due to long-term loading, and temperature effects were not computed. The interlayer shear modulus  $G_i$  was varied

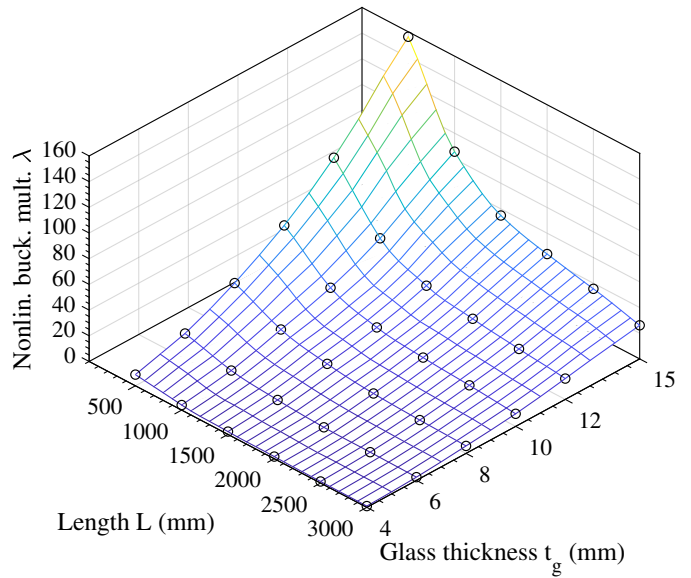


**Fig. 11.** Nonlinear buckling multipliers for in-plane loading: effect of side length and glass thickness.

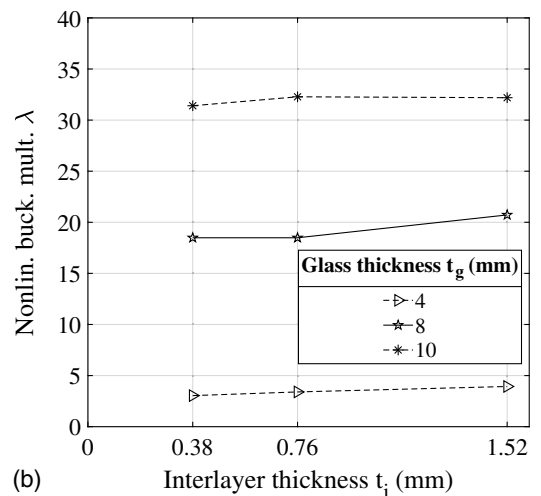
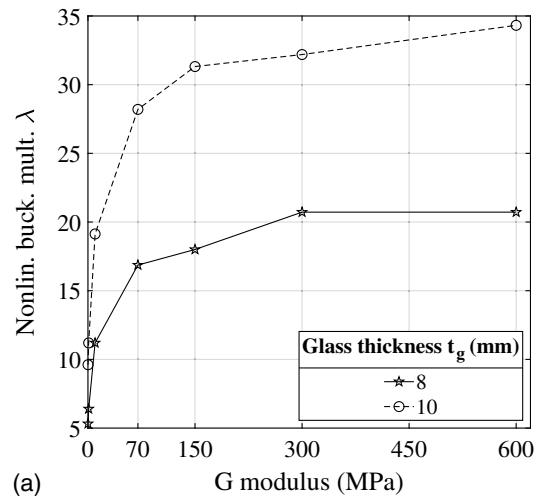


**Fig. 12.** Nonlinear buckling multipliers for in-plane loading: effect of (a) interlayer stiffness; and (b) interlayer thickness.

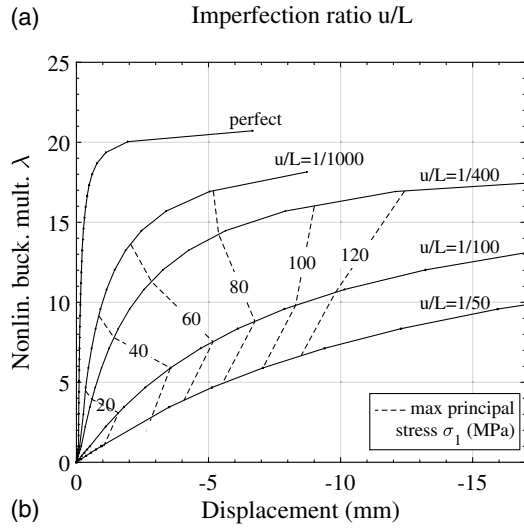
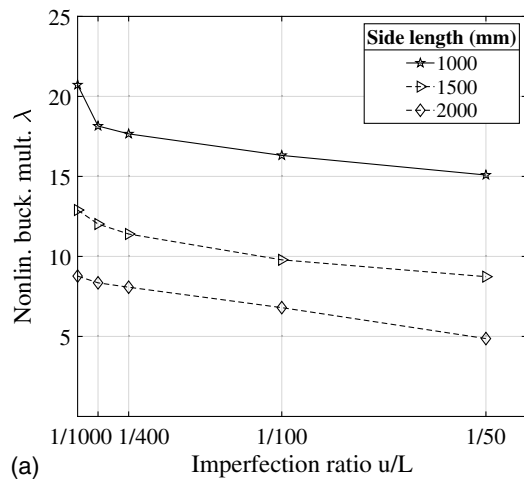


**Fig. 13.** Nonlinear buckling multipliers for in-plane loading: (a) effect of imperfection ratio; and (b) maximum principal stress domain for the 1,000-mm-sided panel.

from the reference value of 300 MPa, while Poisson's coefficient was kept invariant at  $\nu = 0.45$ .

As can be seen from Fig. 12(a), despite the balancing of compression forces demanded by the in-plane stiff glass panels, the weakest composite effect obtained for the lowest values of the  $G_i$  modulus produced a noticeable decrease in the buckling multiplier. This effect was heightened by the panel dead load in the posttensioning phase. Increasing the  $G_i$  modulus from the reference value of 300 to 600 MPa seemed not to affect the panel's out-of-plane response, even when the monolithic limit was reached. Conversely, decreasing the  $G_i$  modulus led to a loss of 18% at  $G_i = 70$  MPa for the 8-mm panel (12% for the 10-mm panel) and a loss of 74% at  $G_i = 0.1$  MPa (70% for the 10-mm panel). Although there was no apparent advantage to selecting an interlayer stiffer than 300 MPa, its choice was justified in terms of viscosity sensitivity. There was a risk of premature panel buckling if the interlayer stiffness dangerously decayed with long-term loading and increasing temperature. This aspect needs to be carefully considered in the design phase.

#### Effect of Interlayer Thickness

Fig. 12(b) shows that the thickness of the interlayer with 300-MPa stiffness had only a minor influence on the out-of-plane buckling of a 1,000-mm-sided panel. This result did not alter even when

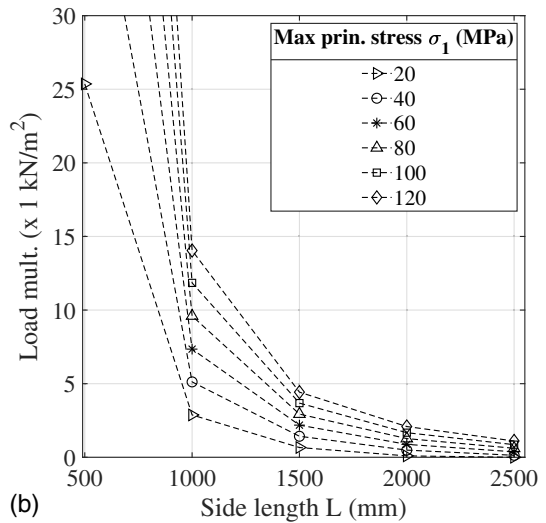
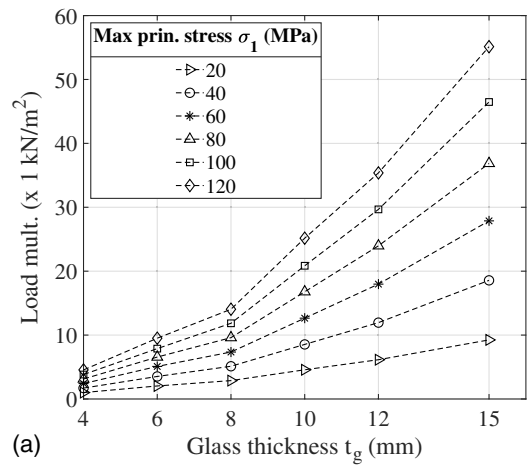


**Fig. 14.** Nonlinear out-of-plane loading: effect of (a) glass thickness; and (b) side length.

the thickness of the component laminated panels varied. The ideal interpolating line was roughly constant. Because any value can be chosen as the best interlayer thickness, the choice should be based on detailed studies of postbreakage behavior.

#### Effect of Initial Imperfection

The effect of geometrical imperfections in glass panels is shown in Fig. 13(a). Parabolic imperfections led to the lowest buckling multipliers, so only their output is represented. Although the panel was bent out of plane because of the dead load applied in Phase 1, yielding generally conservative values for the final multipliers, the imperfection amplitude had a noticeable influence on the structural response. For imperfection ratio values lower than  $L/400$ , the buckling multiplier decreased exponentially, while for high values it decreased linearly. The more slender the panel, the less sensitive it was to imperfections, especially within the imperfection ratio range of 0–400. Thus the 2,000-mm-sided panel interpolating line can be regarded as an almost linear function.

The effect of imperfection on failure mode was considerable. The fracture of a panel without imperfections occurred with progressive buckling, and no noticeable tensile stresses arose until the snap-through multiplier was reached. Because of out-of-plane imperfections, such a configuration suffered from bending stress increased by in-plane loading. Consequently, tensile stress peaks

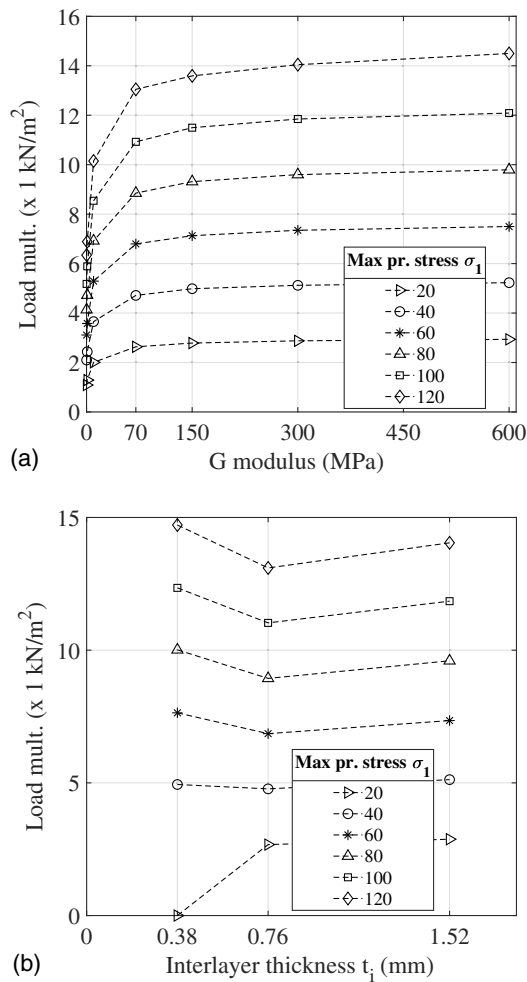


**Fig. 15.** Nonlinear out-of-plane loading: effect of (a) interlayer stiffness; and (b) interlayer thickness.

appeared at the upper panel border line between the clamping area and the free surface, causing tensile failure to precede compression buckling. Fig. 13(b) shows the in-plane load multiplier versus out-of-plane displacement obtained for the reference panel by varying

the initial imperfection amplitude. For larger imperfections, major values for maximum principal stress occurred with lower load multipliers.

### Out-of-Plane Loading

#### Effect of Glass Thickness

Bending stress affected the panel in the out-of-plane loading of Phase 2. The highest tensile values normally occurred in the upper panel adjacent to the Corner-A clamping [Fig. 6(a)] because the effect of precompression was minor away from the main compression line (Edge BC).

The influence of glass thickness on tensile stresses could be regarded as an exponential function of the out-of-plane multiplier or a bilinear with a shifting point at the abscissa of 8 mm. Even though panels thicker than 8 mm can withstand common wind pressures or snow loading, it appears that thinner panels cannot. Indeed, high stresses were reached for limited values of load multipliers. The stress isolines spread out with glass thickness [Fig. 14(a)].

#### Effect of Side Length

Side length had a great influence on the panel's mechanical response as shown in Fig. 14(b). For this reason, the multiplier axis value was limited to 30 in order to improve the readability of larger panel values. The 3,000-mm-sided panel is not been represented because of its lack of appreciable bending strength. A decreasing exponential tendency described the effect of length. Because the high slope of such curves was also due to major loaded areas associated with larger panels, the stress isolines came closer with increasing panel length.

#### Effect of Interlayer Stiffness

The effect of interlayer stiffness on out-of-plane-loading shown in Fig. 15(a) is similar to that shown in Fig. 12(a). The stress isolines are rapidly decreasing for lower interlayer shear moduli. Values for the  $G_i$  modulus higher than 70 MPa lead to roughly linear interpolating lines: almost constant for lower stress isolines and slightly sloped for higher ones. For values lower than 70 MPa, the laminated panel approaches its layered limit and the stresses on the glass reach high values more rapidly.

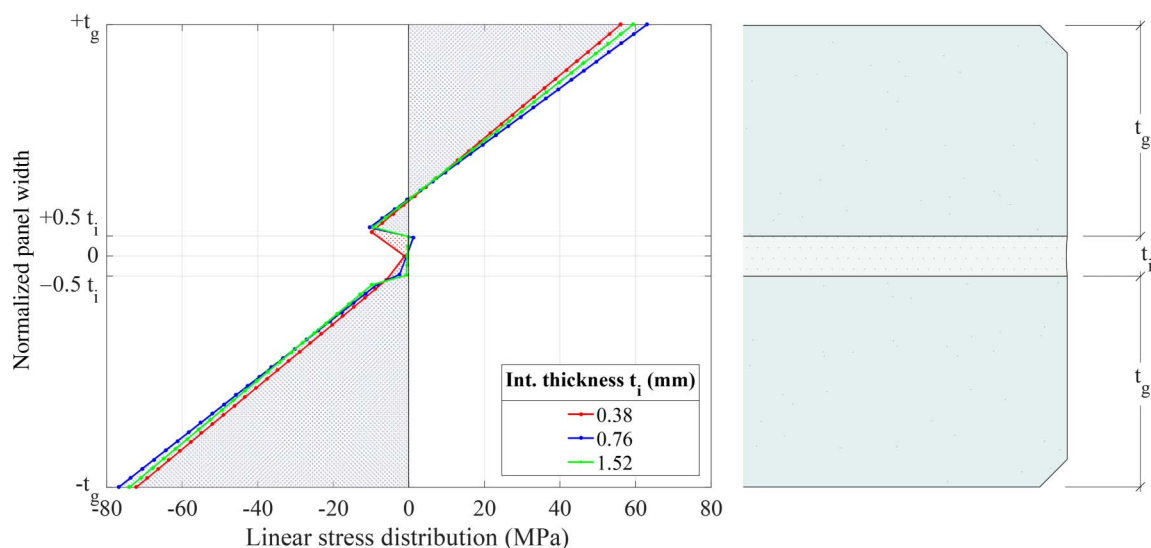


**Fig. 16.** Schematic of normal stress distribution at boundary of Corner A: effect of interlayer thickness for the load multiplier  $\alpha = 9.0$ .

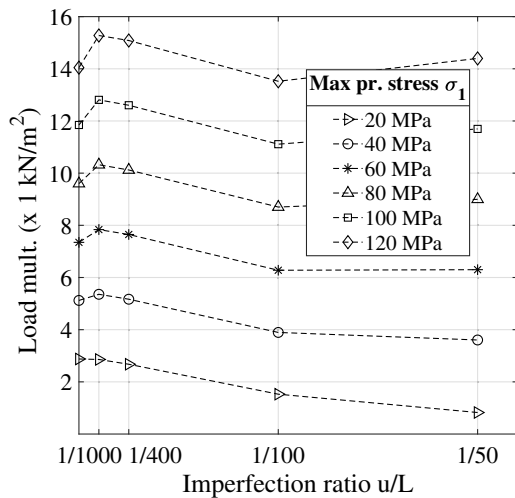


Fig. 17. Nonlinear out-of-plane loading: effect of imperfection ratio.

### Effect of Interlayer Thickness

Interlayer thickness  $t_i$  played a greater role in out-of-plane behavior, as shown in Fig. 15(b). In particular, major panel stiffness is observed for the 0.38-mm-thick interlayer because, given its limited dimension, the behavior of the panel is close to the monolithic limit. The less stiff panel in the three tested models has a 0.76-mm-thick interlayer, while the load multiplier increases to a thickness of 1.52 mm. The latter has still lower stiffness with respect to the 0.38-mm panel, so the monolithic limit is not reached but is larger than the 0.76-mm panel because of the major distance between the glass plates. To confirm this difference stiffness, Fig. 16(a) compares the three in a plot representing normal stress for the same load multiplier  $\alpha = 9$ . Despite this  $\alpha$  value being quite high, a slight predominance of compression stresses highlights the benefits of posttensioning.

### Effect of Initial Imperfection

Initial imperfection appeared to have a beneficial effect on the stress levels of the out-of-plane-loaded panels, probably because of inherent shape resistance as shown in Fig. 17. Ideal interpolating isolines present a local maximum at  $u = L/400$  imperfection amplitude and then decrease with higher values. The lower stress lines are flatter than the higher stress lines.

## Conclusions

Parametric nonlinear FE investigations were carried out on laminated triangular glass panels with rounded edges in a hybrid glass-steel system. Mechanical and geometrical parameters were studied to evaluate their effect on the panels' structural responses. The posttensioned panels were shown to have relevant and uncharted potential in long-span and tall structures.

The results show that the geometrical parameters of panel length and thickness have maximum effect on both in-plane and out-of-plane behavior. As for the mechanical parameters, it was shown that, if the interlayer shear modulus is lower than 70 MPa, the panel exhibits major stiffness decay; if lower than 150 MPa (soft interlayer), the panel is more inclined to buckle.

Imperfection also affects panel response. In the earliest phases of the study, the parabola was observed to be the most severe imperfection shape. The more slender the in-plane-loaded panel, the greater its sensitivity to imperfection amplitude. On the other hand, as in the out-of-plane loading phase, imperfections seemed not to

deeply affect stiffness. However, dead load deformation (Phase 1 of loading), albeit small, acting as a kind of geometrical imperfection, is always present.

Interlayer thickness has a small effect on panel statics. Because no criteria emerged from this parametric study, the selection of thickness can be better determined via postbreakage behavior, which was not covered in this research.

The research findings provide reference values for the design of hybrid spatial triangulated structures. Full-scale experiments will have to be performed that carefully evaluate imperfection (both shape and amplitude), deviation from glass nominal thicknesses, and long-term loading and temperature. Where appropriate, possible strategies to improve in- or out-of-plane behavior are increasing node stiffness and providing additional (punctual or continuous) edge restraints so as not to magnify the panel's self-weight.

## References

- Amadio, C., and C. Bedon. 2010. "Buckling of laminated glass elements in compression." *J. Struct. Eng.* 137 (8): 803–810. [https://doi.org/10.1061/\(ASCE\)ST.1943-541X.0000328](https://doi.org/10.1061/(ASCE)ST.1943-541X.0000328).
- Bedon, C., and C. Louter. 2016. "Finite-element analysis of post-tensioned SG-laminated glass beams with mechanically anchored tendons." *Glass Struct. Eng.* 1 (1): 39–59. <https://doi.org/10.1007/s40940-016-0020-7>.
- Bedon, C., and C. Louter. 2017. "Finite element analysis of post-tensioned SG-laminated glass beams with adhesively bonded steel tendons." *Compos. Struct.* 167 (May): 238–250. <https://doi.org/10.1016/j.compstruct.2017.01.086>.
- Belis, J., D. Mocibob, A. Luible, and M. Vandebroek. 2011. "On the size and shape of initial out-of-plane curvatures in structural glass components." *Constr. Build. Mater.* 25 (5): 2700–2712. <https://doi.org/10.1016/j.conbuildmat.2010.12.021>.
- CNR (Consiglio Nazionale delle Ricerche). 2011. *Istruzioni per la Progettazione, l'Esecuzione ed il Controllo di Strutture di Alluminio*. CNR DT 208/2011. Rome: CNR.
- Cupać, J., K. Martens, A. Nussbaumer, J. Belis, and C. Louter. 2017. "Experimental investigation of multi-span post-tensioned glass beams." *Glass Struct. Eng.* 2 (1): 3–15. <https://doi.org/10.1007/s40940-017-0038-5>.
- Eastman. 2017. "Product information bulletin Saflex® DG structural interlayer." Accessed April 2, 2017. [http://www.mepla.eu/media/medien/product-technical-sheet---saflex-dg\\_060415\\_9ab18.pdf](http://www.mepla.eu/media/medien/product-technical-sheet---saflex-dg_060415_9ab18.pdf).
- Ebert, J. 2014. "Einleitung hoher Lasten in Glaskanten: Ein Beitrag zum Einsatz von Kunststoffen als Klotzungsmaterial." Ph.D. thesis, Saechsische Landesbibliothek-Staats- und Universitaetsbibliothek Dresden.
- Engelmann, M., and B. Weller. 2016. "Post-tensioned glass beams for a 9 m spannglass bridge." *Struct. Eng. Int.* 26 (2): 103–113. <https://doi.org/10.2749/101686616X14555428759000>.
- Englhardt, O. 2007. "Flächentragwerke aus Glas—Tragverhalten und Stabilität." Ph.D. thesis, Univ. of Natural Resources and Life Sciences.
- Englhardt, O., and K. Bergmeister. 2005. "Structural behaviour of plane glass surface structures under compression stress—Numerical and experimental investigation." In *Proc., Glass Processing Days*. Tampere, Finland: Glaston Finland.
- Feng, R. Q., Y. Jihong, and Y. A. Yao. 2015. "New type of structure: Glass cable truss." *J. Bridge Eng.* 20 (12): 04015024. [https://doi.org/10.1061/\(ASCE\)BE.1943-5592.0000734](https://doi.org/10.1061/(ASCE)BE.1943-5592.0000734).
- Froli, M., and F. Laccone. 2018a. "Hybrid glass-steel stele (HYGLASS): Preliminary mechanical study on a smart tetrahedral cantilevering tall structure." In Vol. 6 of *Proc. Challenging Glass Conf.*, 611–616. Delft, Netherlands: TU Delft Open.
- Froli, M., and F. Laccone. 2018b. "HYGLASS: Design proposal for an integrated multifunctional hybrid glass-steel structure." *Int. J. Struct. Glass Adv. Mater. Res.* 2: 15–21. <https://doi.org/10.3844/sgamrsp.2018.15.21>.

- Froli, M., and F. Laccone. 2018c. "Static concept for long-span and high-rise glass structures." *J. Archit. Eng.* 24 (1): 04017030. [https://doi.org/10.1061/\(ASCE\)AE.1943-5568.0000285](https://doi.org/10.1061/(ASCE)AE.1943-5568.0000285).
- Froli, M., F. Laccone, and D. Maesano. 2017. "The TVT glass pavilion: Theoretical study on a highly transparent building made with long-spanned TVT portals braced with hybrid glass-steel panels." *Build.* 7 (4): 50. <https://doi.org/10.3390/buildings7020050>.
- Froli, M., and L. Lani. 2010. "Glass tensegrity trusses." *Struct. Eng. Int.* 20: 436–441. <https://doi.org/10.2749/101686610793557564>.
- Froli, M., and V. Mamone. 2014. "A 12 meter long segmented, post-tensioned steel-glass beam (TVT Gamma)." In *Proc., Challenging Glass 4 and COST Action TU0905 Final Conf.*, 243–251. Rotterdam, Netherlands: A.A. Balkema.
- Froli, M., G. Masiello, A. Melis, V. Mamone, and M. Giammattei. 2014. "The Energy Gallery: A pilot project in Pisa." In *Proc., Engineered Transparency. Int. Conf. at Glasstec*, 621–628. Pisa, Italy: Univ. of Pisa.
- Fuller, R. B. 1982. *Synergetics: Explorations in the geometry of thinking*. San Francisco: Estate of R. Buckminster Fuller.
- Haarhuis, K., and T. Wever. 2016. "Glass-reinforced steel structures." *Glass Struct. Eng.* 1 (1): 195–203. <https://doi.org/10.1007/s40940-016-0021-6>.
- Haldimann, M., A. Luible, and M. Overend. 2008. *Structural use of glass*. Zürich: International Association for Bridge and Structural Engineering.
- Huveners, E. M. P., F. Van Herwijnen, F. Soetens, and H. Hofmeyer. 2007. "Glass panes acting as shear wall." *Heron* 52 (1/2): 5.
- Ioannis, S. M., D. Simon, S. Nhamoinesu, and M. Overend. 2012. "Investigation of double-layer tensegrity glazing systems." In *Proc., IASS Annual Symp.—IASS-APCS 2012*, Seoul.
- Jordão, S., M. Pinho, J. P. Martin, A. Santiago, and L. C. Neves. 2014. "Behaviour of laminated glass beams reinforced with pre-stressed cables." *Steel Constr.* 7 (3): 204–207. <https://doi.org/10.1002/stco.201410027>.
- Kappraff, J. 2001. Vol. 25 of *Connections: The geometric bridge between art and science*. Singapore: World Scientific.
- Kuraray Europe. 2017. "Bulletin edition 2: Kuraray structural and security glazing products—Making glass stronger." Accessed April 2, 2017. [https://www.trosifol.com/fileadmin/user\\_upload/TROSIFOL/support/downloads/bulletin/Bulletin\\_StructGlazing\\_4\\_2017\\_engl\\_web.pdf](https://www.trosifol.com/fileadmin/user_upload/TROSIFOL/support/downloads/bulletin/Bulletin_StructGlazing_4_2017_engl_web.pdf).
- Louter, C., J. Belis, F. Veer, and J. P. Lebet. 2012. "Structural response of SG-laminated reinforced glass beams; experimental investigations on the effects of glass type, reinforcement percentage and beam size." *Eng. Struct.* 36 (Mar): 292–301. <https://doi.org/10.1016/j.engstruct.2011.12.016>.
- Louter, C., J. Cupac, and J. P. Lebet. 2014. "Exploratory experimental investigations on post-tensioned structural glass beams." *J. Facade Des. Eng.* 2 (1–2): 3–18. <https://doi.org/10.3233/FDE-130012>.
- Mamone, V. 2015. "Experimental, numerical and analytical investigations on the segmented post-tensioned hybrid steel-glass beams TVT." Ph.D. thesis, Dept. of Civil Engineering, Univ. of Pisa.
- Martens, K., R. Caspeele, and J. Belis. 2015a. "Development of composite glass beams—A review." *Eng. Struct.* 101 (Oct): 1–15. <https://doi.org/10.1016/j.engstruct.2015.07.006>.
- Martens, K., R. Caspeele, and J. Belis. 2015b. "Development of reinforced and posttensioned glass beams: Review of experimental research." *J. Struct. Eng.* 142 (5): 04015173. [https://doi.org/10.1061/\(ASCE\)ST.1943-541X.0001453](https://doi.org/10.1061/(ASCE)ST.1943-541X.0001453).
- Martens, K., R. Caspeele, and J. Belis. 2016a. "Load-carrying behaviour of interrupted statically indeterminate reinforced laminated glass beams." *Glass Struct. Eng.* 1 (1): 81–94. <https://doi.org/10.1007/s40940-016-0017-2>.
- Martens, K., R. Caspeele, and J. Belis. 2016b. "Numerical investigation of two-sided reinforced laminated glass beams in statically indeterminate systems." *Glass Struct. Eng.* 1 (2): 417–431. <https://doi.org/10.1007/s40940-016-0005-6>.
- Memari, A. M., R. A. Behr, and P. A. Kremer. 2003. "Seismic behavior of curtain walls containing insulating glass units." *J. Archit. Eng.* 9 (2): 70–85. [https://doi.org/10.1061/\(ASCE\)1076-0431\(2003\)9:2\(70\)](https://doi.org/10.1061/(ASCE)1076-0431(2003)9:2(70)).
- Mocibob, D. 2008. "Glass panel under shear loading." Ph.D. thesis, École Polytechnique Fédérale de Lausanne.
- Pottmann, H. 2007. Vol. 10 of *Architectural geometry*. Exton, PA: Bentley Institute Press.
- Silvestru, V., M. Zellinger, and O. Enghardt. 2013. "Hybrid glass structures for building skins—Actions and requirements." In *Proc., COST Action TU0905 Mid-Term Conf. on Structural Glass*, 33–42. London: CRC Press.
- Sobek, W. 2007. "Strutture in vetro." *Swiss Rev. Archit. Eng. Urban Plann.*
- Stepinac, M., V. Rajčić, L. Krstevska, and L. Tashkov. 2013. "Simulation of earthquake load imposed on timber—Glass composite shear wall panel." In *Proc., COST Action TU0905 Mid-term Conf. on Structural Glass*, 245–252. Rotterdam, Netherlands: A.A. Balkema.
- Štrukelj, A., B. Ber, and M. Premrov. 2015. "Racking resistance of timber-glass wall elements using different types of adhesives." *Constr. Build. Mater.* 93 (Sep): 130–143. <https://doi.org/10.1016/j.conbuildmat.2015.05.112>.
- Weller, B., S. Reich, and J. Ebert. 2008. "Testing on space grid structures with glass as compression layer." In *Proc., Challenging Glass Conf.*, 155–162. Amsterdam, Netherlands: IOS Press.
- Weller, B., S. Reich, and J. Ebert. 2010. "Transparentes Raumstabwerk über dem Innenhof des Berliner Reichstagspräsidentenpalais." Supplement, *Stahlbau* 79 (S1): 3–9. <https://doi.org/10.1002/stab.201001301>.
- Weller, B., S. Reich, J. Ebert, and P. Krampe. 2009. "Testing for individual approval of a vault roof with in-plane loaded glass panes." In *Proc., Int. Association for Shell and Spatial Structures (IASS) Symp. 2009*, 2990–3001. Valencia, Spain: Editorial Universitat Politècnica De Valencia.
- Wellershoff, F. 2006. "Nutzung der Verglasung zur Aussteifung von Gebäudehüllen." Ph.D. thesis, RWTH Aachen.